

From Field to Sky: Measurement and Modeling of Transgenic Switchgrass Pollen Dispersal in the Atmosphere

Manu Nimmala

Virginia Tech

Hope A. Gruszewski

Virginia Tech

Regina Hanlon

Virginia Tech

Landon Bilyeu

Virginia Tech

Tyler Newton

University of Tennessee at Knoxville

Jessica Stockdale

University of Tennessee at Knoxville

Reginald J. Millwood

University of Tennessee at Knoxville

Charles N. Stewart

University of Tennessee at Knoxville

Craig Powers

Virginia Tech

Shane D. Ross

Virginia Tech

Hosein Foroutan

Virginia Tech

David G. Schmale

dschmale@vt.edu

Virginia Tech

Research Article

Keywords: switchgrass, transgenic, pollen dispersal, bioaerosol, drone sampling, pollen transport, fluorescence

Posted Date: March 9th, 2026

DOI: <https://doi.org/10.21203/rs.3.rs-8768887/v1>

License: © ⓘ This work is licensed under a Creative Commons Attribution 4.0 International License.

[Read Full License](#)

Additional Declarations: No competing interests reported.

1 From Field to Sky: Measurement and Modeling of
2 Transgenic Switchgrass Pollen Dispersal in the
3 Atmosphere

4 Manu Nimmala¹, Hope A. Gruszewski², Regina Hanlon²,
5 Landon Bilyeu², Tyler Newton⁵, Jessica Stockdale⁵,
6 Reginald J. Millwood⁵, Charles N. Stewart⁵, Craig Powers²,
7 Shane D. Ross³, Hosein Foroutan⁴, David G. SchmaleIII^{2*}

8 ¹Mechanical Engineering, Virginia Tech, Blacksburg, 24061, VA, USA.

9 ²School of Plant and Environmental Sciences, Virginia Tech,
10 Blacksburg, 24061, VA, USA.

11 ³Aerospace and Ocean Engineering, Virginia Tech, Blacksburg, 24061,
12 VA, USA.

13 ⁴Civil and Environmental Engineering, Virginia Tech, Blacksburg,
14 24061, VA, USA.

15 ⁵Department of Plant Sciences, University of Tennessee, Knoxville,
16 37996, TN, USA.

17 *Corresponding author(s). E-mail(s): dschmale@vt.edu;

18 Contributing authors: nimmala@vt.edu; anon47@vt.edu;

19 rhanlon@vt.edu; bilyeu@vt.edu; cnewto12@vols.utk.edu;

20 jstockdale0303@icloud.com; rmillwood@utk.edu; nealstewart@utk.edu;

21 craigwpowers@craigsci.com; sdross@vt.edu; hosein@vt.edu;

22 **Abstract**

23 Accurate tracking and measurement of pollen dispersal in the atmosphere are
24 essential for assessing cross-pollination risks, particularly in the case of genetically
25 engineered (GE) crops. We conducted a series of unique release-recapture field
26 studies with GE switchgrass in Oliver Springs, Tennessee, USA. Two hundred
27 transgenic switchgrass plants (*Panicum virgatum* L. ‘Performer’) were planted at
28 the center of a clear-cut field, with one block of 100 plants expressing orange fluo-
29 rescent protein (OFP) under a maize ubiquitin promoter (PvUBI1) and another
30 block of 100 plants expressing OFP driven by a maize pollen-specific promoter

31 (Zm13). Pollen was sampled from the atmosphere using fixed (ground-based) and
32 mobile (drone-based) sampling devices at different distances from the source field,
33 with Lagrangian Stochastic dispersal simulations run for sampling periods using
34 high-resolution wind measurements. The pollen emission rate was estimated by
35 combining simulated and measured pollen concentrations, and strong diurnal
36 trends were observed. Diurnal emission rate trends were positively correlated
37 with wind speed, temperature, and vapor pressure deficit, while negatively corre-
38 lated with relative humidity. In low-wind meandering conditions, incorporating
39 changing wind direction into the dispersal modeling improved pollen emission
40 rate estimation and model-measurement comparisons. This study assesses the
41 effectiveness of high and low volume pollen samplers in relation to source strength
42 up to 1 km from the source, enhancing understanding of pollen measurement
43 techniques. Additionally, it is a proof-of-concept for drone-based pollen sampling
44 and GMO pollen tracking using fluorescence measurements. Results from our
45 experiments have significant implications for cross-pollination risk assessment,
46 prediction, and management of airborne allergens.

47 **Keywords:** switchgrass, transgenic, pollen dispersal, bioaerosol, drone sampling,
48 pollen transport, fluorescence

49 1 Introduction

50 Accurate tracking and measurement of pollen dispersal in the atmosphere are impor-
51 tant for assessing cross-pollination risks (Aylor et al. 2003; Nimmala et al. 2024),
52 particularly in the case of genetically engineered (GE) crops. Wind-dispersed pollen
53 is the primary method of gene flow in many grasses, including switchgrass (*Panicum*
54 *virgatum*), an important bioenergy crop (Sofiev and Bergmann 2012). It is a peren-
55 nial, warm-season C4 bunchgrass found across most of eastern North America—from
56 northern Mexico to southern Canada. Originally adopted as a forage crop, it is now
57 a leading candidate for large-scale lignocellulosic biofuel feedstock in the U.S. and
58 beyond (Parrish and Fike 2005). There is increasing concern that the rapid growth and
59 development of switchgrass as a biofuel could result in gene flow from GE switchgrass
60 fields to nontransgenic fields (including wild populations), leading to both financial
61 and ecological damage (Kwit and Stewart 2012; Millwood et al. 2017; Ahrens et al.
62 2011; Ecker et al. 2015; Stockdale and Millwood 2023). These changes could be com-
63 pounded by the effects of climate change, where rising temperatures result in altered
64 native switchgrass territory (Ahrens et al. 2014). Therefore, there is an urgent need for
65 field experiments and modeling efforts to characterize the dispersal of airborne switch-
66 grass pollen in relation to meteorological factors for regulation and risk management
67 purposes.

68 There are limited experimental and modeling studies on switchgrass gene flow
69 (Kwit and Stewart 2012); these model pollen dispersal with and without wind breaks
70 (Auer et al. 2016), experimentally quantify the dispersal and cross-pollination of trans-
71 genic switchgrass (Millwood et al. 2017), and model transport in low and high-wind
72 conditions (Ecker et al. 2013). In 2011, Millwood and colleagues conducted the first

73 regulated transgenic switchgrass field experiments in the U.S. (Millwood et al. 2017).
74 A 3-year field experiment was performed in Oliver Springs, Tennessee, U.S.A. where
75 100 clonal switchgrass ‘Alamo’ plants transgenic for an orange-fluorescent protein
76 (OFP) were used as the pollen source (whole plants, including pollen, were orange-
77 fluorescent). To assess pollen movement, pollen traps were placed at 10 m intervals
78 from the pollen-source plot in the four cardinal directions extending up 100 m from
79 the field. Results showed that pollen-mediated gene flow is likely to occur over dis-
80 tances of at least 100 m (Millwood et al. 2017). This study provided important baseline
81 data useful to determine isolation distances and other management practices, should
82 transgenic switchgrass be grown commercially in relevant environments. Since switch-
83 grass is an obligate outcrossing perennial grass, there are concerns about gene flow
84 and the need for bioconfinement, especially for pollen (Kausch et al. 2010; Kwit and
85 Stewart 2012; Stockdale and Millwood 2023). Moreover, since North America is the
86 geographic center of switchgrass diversity, a better understanding of pollen movement
87 in this species is needed (Kwit and Stewart 2012).

88 The spread of pollen through the atmosphere involves processes of liberation, drift,
89 and deposition (Aylor et al. 2003; Isard and Gage 2001). Knowledge of these processes
90 can help growers and producers make informed management decisions regarding pollen
91 transport in seed production fields and neighboring farms (Isard and Gage 2001).
92 Although atmospheric transport models can predict pollen movement, they often fail
93 to incorporate actual measurements of pollen concentrations and viability. Various
94 unmanned aircraft systems (UASs or drones) have previously been used to detect and
95 monitor pollen movement over long distances in the lower atmosphere. Gottwald and
96 Tedders pioneered the collection of pollen with UASs (Gottwald and Tedders 1985).
97 They modified a remote-controlled biplane platform with two rotating drum samplers
98 to collect pollen and plant pathogen spores over pecan and peach orchards. Their
99 study demonstrated the significant potential for regional-scale transport of pollen and
100 plant pathogens among orchards. Two decades later, Aylor and colleagues (Aylor
101 et al. 2006) combined ground-based sampling devices with UASs to collect pollen
102 within and above a cornfield. Over the past decade, Schmale and colleagues have
103 integrated autonomous systems into UASs, enabling teams of vehicles to coordinate
104 flight missions and perform complex atmospheric sampling tasks (Schmale III et al.
105 2008; Techy et al. 2010).

106 The allergen-management community needs a fast and reliable sensor network to
107 measure airborne pollen concentrations to enable timely and accurate allergen report-
108 ing (Beggs 2024; Buters et al. 2024; Suanno et al. 2021; Tummon et al. 2021). Current
109 allergen information reports only broad species group concentrations, typically at a
110 daily resolution at best (Buters et al. 2018; Tummon et al. 2021). Future airborne
111 pollen forecasts can be enhanced by integrating known pollen emissions with large-
112 scale atmospheric models. Understanding diurnal pollen release patterns could aid in
113 allergen treatment and improve emission source data for potential forecast models
114 (Buters et al. 2018). To our knowledge, most airborne pollen field studies and cor-
115 responding allergen reports rely on Hirst-type samplers (Plaza et al. 2022). These
116 sampling devices are constrained by a relatively low sampling rate of approximately
117 10 L/min (Adamov et al. 2024; Plaza et al. 2022), necessitating either high airborne

118 pollen concentrations or extended sampling durations to accurately characterize pollen
119 levels. The latter constraint contributes to the coarse temporal resolution of daily
120 allergen pollen reporting.

121 We hypothesized that (1) wind-dispersed pollen from switchgrass could be tracked
122 and quantified using orange fluorescent protein (OFP) expression, (2) a Lagrangian
123 Stochastic (LS) dispersal model could estimate pollen source strength in the field,
124 and (3) an array of novel samplers could serve as viable alternatives to standard
125 Hirst-type samplers. To test these hypotheses, we conducted a series of unique release-
126 recapture field studies using GE switchgrass in Oliver Springs, Tennessee, USA. Two
127 hundred plants from five transgenic lines of switchgrass (*Panicum virgatum* L. ‘Per-
128 former’) were planted at the center of a clear-cut field. One block consisted of 100
129 plants expressing OFP under the control of a maize ubiquitin promoter (PvUBI1),
130 while the other block contained 100 plants expressing OFP driven by a maize pollen-
131 specific promoter (Zm13). Pollen from the atmosphere surrounding these blocks of
132 transgenic switchgrass was collected using a series of fixed (ground-based) and mobile
133 (drone-based) sampling devices at various distances from the field center. The efficacy
134 of these various samplers was evaluated within 25 m of the source and up to 1 km
135 from the source. LS dispersal simulations were conducted for pollen sampling periods
136 using high-resolution wind measurements collected near the field. Pollen emission rates
137 were estimated by combining simulated concentrations with field concentration mea-
138 surements. By integrating high-resolution measurements and simulations, our study
139 evaluates the performance of emerging sampling technologies and highlights their
140 implications for biosecurity, allergen tracking, and ecological modeling.

141 2 Materials and Methods

142 Three field campaigns were conducted over the course of two calendar years (2021 and
143 2022) to sample airborne pollen around two blocks of transgenic switchgrass.

144 2.1 Field Site and Pollen Source

145 2.1.1 Field site

146 To assess the transport of wind-dispersed pollen from transgenic switchgrass plants,
147 a two-year field study was conducted under USDA APHIS BRS release permits
148 (21-094-103r and 124-86SS5F1). The experiments were carried out at the Tennessee
149 Agricultural Experiment Station, near the University of Tennessee’s Forest Resources
150 Research and Education Center at the Cumberland Forest Unit in Oliver Springs,
151 Tennessee, USA (36.0483147, -84.4811417).

152 The field site was selected to satisfy the primary requirements for regulatory trans-
153 genic pollen dispersal experiments: isolation and traceable source attribution. It was
154 situated on patch of recently cleared forest land, with felled trees forming a rough glade
155 area. The site provided sufficient open area (~1.5 ha) for switchgrass cultivation and
156 sampler deployment, while heavily forested borders served as a natural barrier that
157 reduced the likelihood of cross-contamination with nearby wild or cultivated switch-
158 grass and limited off-site pollen transport. The field location was intentionally chosen

159 in a remote, concealed area beyond a secured access point, ensuring restricted visibil-
160 ity and access. The field plot measured 13.7 m × 9.1 m, enclosed within a protective
161 15.2 m × 19.8 m fenced perimeter, as shown in Figure 1A. The outer fence was locked
162 to prevent animal intrusion.

163 2.1.2 Transgenic line generation, analysis, and selection

164 Transgenic switchgrass plants expressing OFP were created by genetically engi-
165 neering embryogenic callus derived from switchgrass seeds obtained from Ernst
166 Conservation Seeds, Inc. (Meadville, Pennsylvania, USA). This was achieved through
167 Agrobacterium-mediated transformation (*Agrobacterium tumefaciens* strain EHA105)
168 as detailed in Li and Qu (2011), using one of two binary plasmid constructs.

169 The first plasmid, pANIC10A-OFP (Mann et al. 2012), contained the hygromycin
170 phosphotransferase (hph) selectable marker gene under the control of the switchgrass
171 ubiquitin 2 (PvUbi2) promoter as well as an orange fluorescent protein (OFP) gene
172 pporRFP under the control of the switchgrass ubiquitin promoter (PvUBI1). This
173 promoter drives the expression of OFP in leaves, stems, and pollen.

174 The second plasmid, PSYBIN1a-Zm13-pporRFP, also contained the OFP gene
175 pporRFP under the control of a maize pollen-specific promoter (Zm13). This promoter
176 drives the expression of OFP in the pollen. This construct also contained a second
177 OFP gene mOrangeER under the control of the cauliflower mosaic virus (CaMV) 35S
178 promoter which enable the expression of this OFP in callus and green tissues. In addi-
179 tion, the plasmid also contained the hygromycin phosphotransferase (hph) selectable
180 marker gene under the control of the PvUBI2 promoter. Several transgenic OFP-
181 expressing shoots were recovered from hygromycin selection media (100 mg/L), and
182 once rooted, plants were grown in an environmental-controlled growth room (16/8 h
183 day/night and 24/22°C day/night).

184 To confirm the presence of the OFP gene in the transgenic plants, PCR-screening
185 was performed using primers (forward primer: GCAAAGTGGGGTCAAAGATG;
186 reverse primer: CACCTTCAAGCCCTTCTTTG) designed to amplify a 556 bp frag-
187 ment of the pporRFP gene. PCR-confirmed transgenic plants were moved to a
188 greenhouse and grown (16/8 h day/night and 28/22°C day/night) until flowering. To
189 identify transgenic events expressing OFP in pollen, visual analysis of OFP fluores-
190 cence was conducted on pollen grains from each event using epifluorescent microscopy
191 as described by Rice et al. (2013). Transgenic lines in which all pollen grains exhib-
192 ited OFP expression were propagated in the greenhouse and subsequently used in field
193 experiments.

194 2.1.3 Planting

195 The planted area, less than 0.1 ha, consisted of 20 rows with 20 switchgrass plants
196 per row, totaling 400 transgenic switchgrass plants arranged in a randomized design.
197 These plants were hand-transplanted in the field at 76.2 cm intervals on three different
198 dates. On July 20, 2021, 100 pANIC10A-OFP switchgrass plants from five transgenic
199 events (20 clonal replicates per event) were transplanted. On August 26, 2021, another
200 100 PSYBIN1a-Zm13-pporRFP plants from five transgenic events (20 clonal replicates

201 per event) were transplanted. Lastly, on June 20, 2022, an additional 200 pANIC10A-
 202 OFP switchgrass plants from ten transgenic events (20 clonal replicates per event)
 203 were transplanted in the field plot. These last 200 plants were not mature enough
 204 to produce pollen during the field experiments. Figure 1B illustrates the locations of
 205 these plants and their ages in weeks during the August 2-3, 2022 field experiment.
 206 This experimental design was structured to monitor and analyze the dispersal from
 207 transgenic pollen over time and distance.

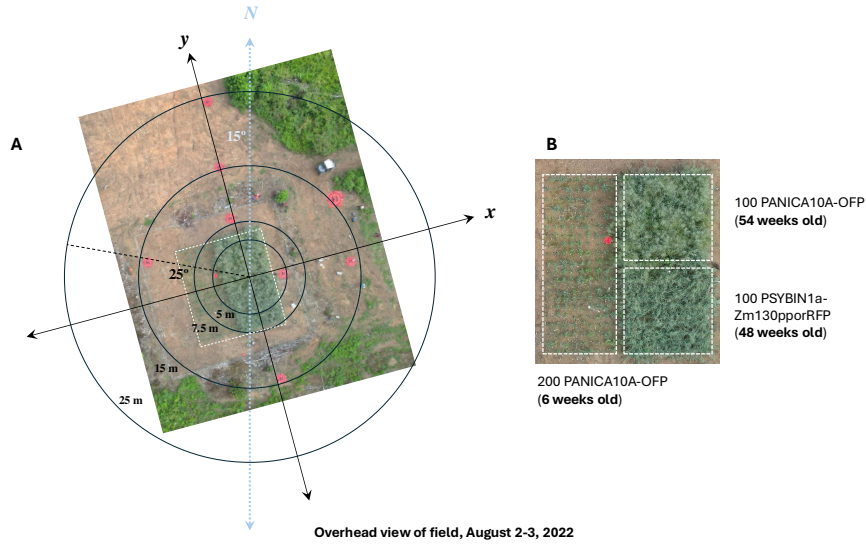


Fig. 1 Top-down drone image of the field during field experiments conducted on August 2-3, 2022. (A) The field of GE switchgrass is outlined by a white dotted square and enclosed by a perimeter fence, as required by the APHIS BRS permits. Reddish-orange circular pads mark the locations of pollen sampling devices, positioned at increasing distances from the center of the source field. (B) A close-up view of the 13.7 m × 9.1 m field of GE Switchgrass, showing the locations of both strains of OFP-expressing switchgrass plants. Labels indicate the plant positions and ages during the August 2-3, 2022, field campaign.

208 2.2 Sampling Methods

209 Four types of volumetric particle samplers, shown in Figure 2, were used to capture
 210 GE switchgrass pollen and estimate the concentration of airborne pollen at various
 211 times and distances from the source field. Each sampler had different sampling rates
 212 and sensing capabilities. To optimize equipment placement, wind forecasts and local
 213 conditions were assessed before the first sampling period. The samplers were strategi-
 214 cally positioned based on prevailing and predicted wind directions, ensuring placement
 215 downwind along the expected pollen dispersal path. Figure 3 illustrates the place-
 216 ment of samplers around the field on each sampling day. The samplers were placed
 217 on reddish-orange circular drone landing pads to mark their locations and enhance

218 visibility in overhead footage, as shown in Figure 1A for the August 2-3, 2022 field
219 campaign.

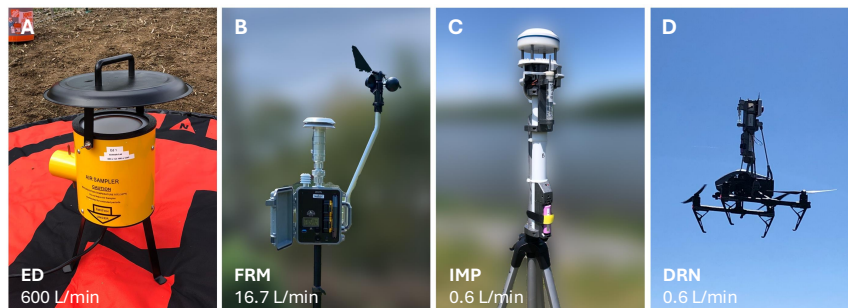


Fig. 2 All sampler units used during the field campaigns. (A) The ED (Science First 2007), a ground-based high-volume sampler (600 L/min). (B) The FRM, a ground-based medium-volume volumetric sampler (16.7 L/min). (C) The IMP, an impinger-based ground-based low-volume sampler (0.6 L/min). (D) The DRN, a drone-based sampler flown at a height of 10 meters above ground level (0.6 L/min).

220 **2.2.1 Ground-based high-volume samplers (ED)**

221 In anticipation of low pollen emission rates, several high-volume filter-based samplers
222 (Science First #15000, Yulee, FL) (Science First 2007) were deployed during the cam-
223 paign (Figure 2A). Originally designed for educational use in schools, these samplers
224 are referred to as “ED” samplers throughout the manuscript.

225 The barrel-shaped ED samplers draw air through a filter surface at an initial flow
226 rate of 600 L/min (Science First 2007). Cellulose filters with a pore size of 11 μm
227 and a diameter of 125 mm were used to collect airborne pollen and other atmospheric
228 particles at 0.432 m above ground level. The ED samplers’ volumetric sampling rate
229 is 1000 times that of the IMP and DRN samplers, and 35 times that of the FRM
230 sampler. This significant increase in sampling capacity allowed for improved detection
231 of airborne pollen, particularly in cases of low pollen emission rates.

232 **2.2.2 Ground-based medium-volume sampler (FRM)**

233 A single near-Federal Reference Method (FRM) sampler (ARA Instruments, Eugene,
234 Oregon) was deployed during the field experiments, shown in Figure 2B. This battery-
235 operated device samples air at a flow rate of 16.7 L/min. The unit is equipped with
236 a filter sampler (PM_{10} filters were used in this study), meteorological sensors, and
237 a particle counter. Additional details about this instrument are available on ARA’s
238 website (ARA Instruments 2016).

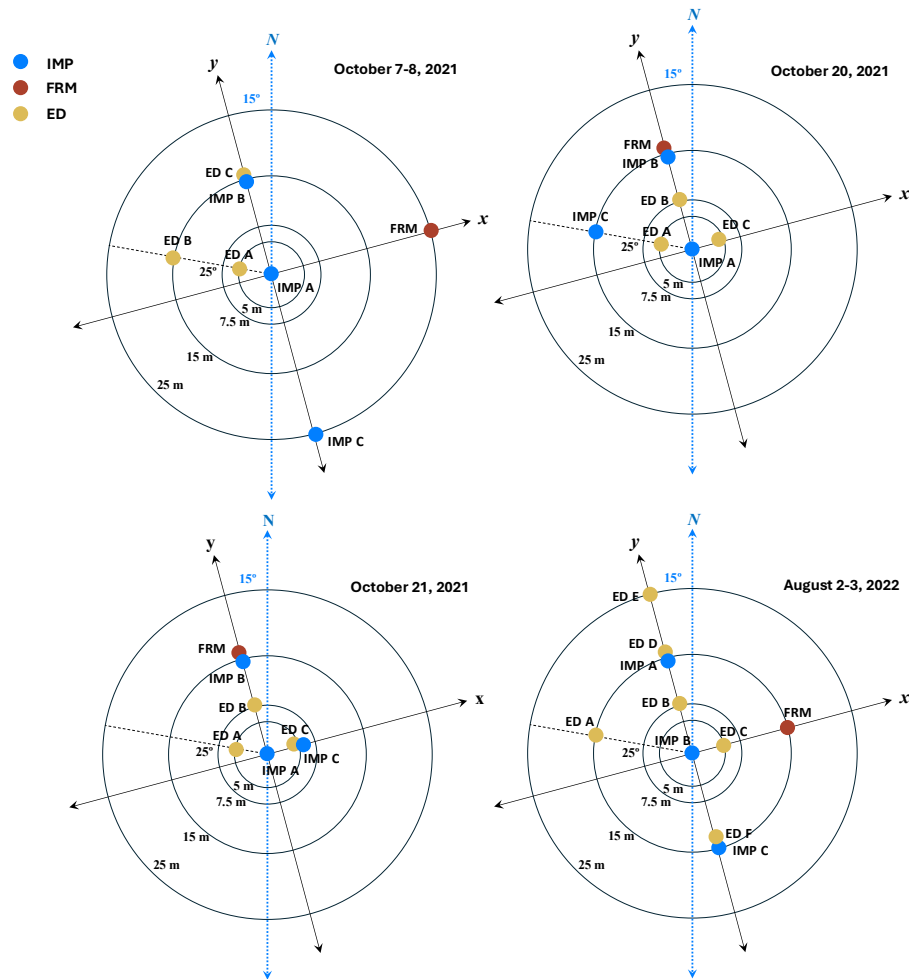


Fig. 3 Ground-based sampler locations for each collection day. Yellow, blue, and red denote placement of ED, IMP, and FRM samplers, respectively, positioned at radial distances of 5, 7.5, 15, and 25 meters from the center of field.

2.2.3 Ground-based low-volume samplers (Impingers or IMP)

To evaluate the effectiveness of impinger-type samplers, three custom-designed impinger packages were deployed during the field campaign (Figure 2C). These sampling packages are referred to as “IMP” throughout the manuscript.

The IMPs were constructed from high-density polyethylene, following the design specifications outlined in Powers et al. (2018). The 3D printing (.stl) files for the impinger units are publicly available online (Powers, C. 2018). These files were modified to accommodate a 15 mL polypropylene conical collection vial (Corning #CLS430791) and a stainless-steel tube with a 4 mm diameter opening.

248 The IMP samplers were mounted on a tripod 2 m above ground level to approxi-
249 mate the height of the switchgrass panicles, the open flower structures that produce
250 pollen. The IMPs sampled airborne particles at a rate of 0.6 L/min, with collected
251 particles entrained in sterile 15 mL conical tubes containing 2 mL of sterile deionized
252 water.

253 **2.2.4 Drone-based low-volume sampler (DRN)**

254 To measure airborne pollen concentration at different altitudes above and downwind of
255 the field, we used a drone-based sampling system consisting of the IMP unit mounted
256 on a DJI Inspire 2 drone platform (Figure 2D). The system is described in detail in
257 [Bilyeu et al. \(2022\)](#).

258 A key design feature of the drone system is the positioning of the IMP sampler high
259 enough above the propellers, which ensures that the sampled air remains free from
260 propeller-induced turbulence, commonly known as downwash. The drone was flown at
261 a fixed altitude of 10 meters during each sampling interval, a height selected to prevent
262 propeller downwash from disturbing the switchgrass canopy during stable hovering.

263 Due to drone battery limitations and the need for safe flight and landing operations,
264 each sampling interval was restricted to 10 minutes. The IMP unit on the drone
265 operated at the same volumetric sampling rate as its ground-based counterpart (0.6
266 L/min). However, because the drone sampler was only flown for 10 minutes per flight,
267 its total sampling capacity was significantly lower than the ground-based IMP units,
268 which collected for 30 to 90 minutes during the field campaign. Hereafter, the IMP-
269 equipped drone system is referred to as “DRN” throughout the manuscript.

270 **2.3 Meteorological Data**

271 A weather station was installed near the field to collect meteorological data throughout
272 each sampling day. The station consisted of a Campbell Scientific CSAT3 three-
273 dimensional sonic anemometer, mounted at a height of 1.5 m above ground level, which
274 measured high-resolution wind velocity in three dimensions and sonic temperature at
275 a frequency of 10 Hz. In addition, a Campbell Scientific HMP45C probe recorded tem-
276 perature and relative humidity every 30 seconds. Meteorological data were recorded
277 with the Campbell Scientific CR3000 datalogger. To minimize interference from the
278 tripod pole, the sonic anemometer arm was positioned perpendicular to the antici-
279 pated dominant wind direction before each collection day. The wind velocities in the
280 u and v directions (relative to the sonic anemometer arm) were then rotated into the
281 cardinal coordinate system for analysis.

282 **2.4 Processing of pollen samples**

283 **2.4.1 Sample preparation**

284 Filters from the ED samplers were processed as shown in Figure 4A. Briefly, the 125
285 mm “ED” collection filters were removed with forceps and transferred to separate
286 150 mm petri dishes (Fisher #FB0875714) in the field immediately following each
287 sampling period. For each filter, 25 mL of 25% EtOH was added in the petri dish,

288 the filter was gently agitated with a sterile cell spreader, and then rinsed a total
289 of 8 times. Each rinsate was transferred by a pipettor to a vacuum filtration unit
290 (Thomas Scientific #300-4100) containing a 47 mm Isopore polycarbonate 10 μm filter
291 (Millipore Sigma #TCTP04700). The sample was cleared through the filter using the
292 vacuum from a hand pipetting bulb. Using forceps, the Isopore filter was then moved
293 to a 60 mm petri dish (Genesee 32-105) and rinsed 6 times with 2 mL 25% EtOH.
294 The resulting rinsate was transferred to an Ultrafree 5 μm PVDF centrifugal filtration
295 tube (Millipore Sigma UFC40SV25) and centrifuged for 2 minutes at 2,500 rpm in a
296 swinging bucket centrifuge (IEC Clinical Centrifuge). The concentrated sample was
297 then resuspended from the 5 μm filter surface with 200 μL 25% EtOH and moved to
298 a 1.5 mL Eppendorf tube and stored at 4 °C for further analysis.

299 Filters from the FRM sampler were processed as shown in Figure 4B. Briefly, the
300 Isopore filter was removed from the FRM unit sampling cartridge using forceps and
301 transferred to a 60 mm petri dish (Genesee 32-105) in the field immediately following
302 each sampling period. For processing the sample, the Isopore filter was then rinsed 6
303 times with 2 mL 25% EtOH, and the resulting rinsate was moved to an Ultrafree 5
304 μm PVDF centrifugal filtration tube and centrifuged for 2 minutes at 2,500 rpm in
305 a swinging bucket centrifuge (IEC Clinical Centrifuge). The concentrated sample was
306 then resuspended from the 5m filter surface with 200 μL of 25% EtOH and moved to
307 a 1.5 mL Eppendorf tube and stored at 4 °C for further analysis.

308 The fluid from the IMP and DRN samplers was processed as shown in Figure
309 4C. Samples from the IMPs and DRN were transferred by pipette to an Ultrafree 5
310 μm PVDF centrifugal filtration tube and centrifuged for 2 minutes at 2,500 rpm in
311 a swinging bucket centrifuge (IEC Clinical Centrifuge). The concentrated sample was
312 then resuspended from the 5 μm filter surface with 200 μL 25 EtOH and transferred
313 to a 1.5 mL Eppendorf tube and stored at 4 °C for further analysis.

314 2.4.2 Pollen counting

315 Switchgrass pollen was counted in each concentrated sample by pipetting the samples
316 into individual wells of a 96-well plate (Grenier Bio One 7000124). Samples were
317 allowed to sediment for 15 minutes and then were observed using an Olympus CKX53
318 inverted microscope equipped with the Olympus EP50 digital camera and associated
319 software. Following the quantification of the switchgrass pollen in each of the tubes,
320 the samples were transferred back into their respective 1.5 mL Eppendorf storage
321 tubes and held at 4 °C for transport and further analysis.

322 2.5 Atmospheric dispersal modeling

323 2.5.1 Meteorological Inputs

324 Atmospheric dispersal simulations for each sampling interval were driven using time-
325 averaged wind statistics collected during that interval. Most sampling intervals
326 occurred under low-wind conditions (< 2 m/s), characterized by meandering winds
327 with frequent directional shifts and intermittent lulls in wind speed. To better cap-
328 ture dispersal dynamics under these conditions, the wind data were processed using
329 different averaging window sizes. Specifically, for the 45-minute sampling intervals on

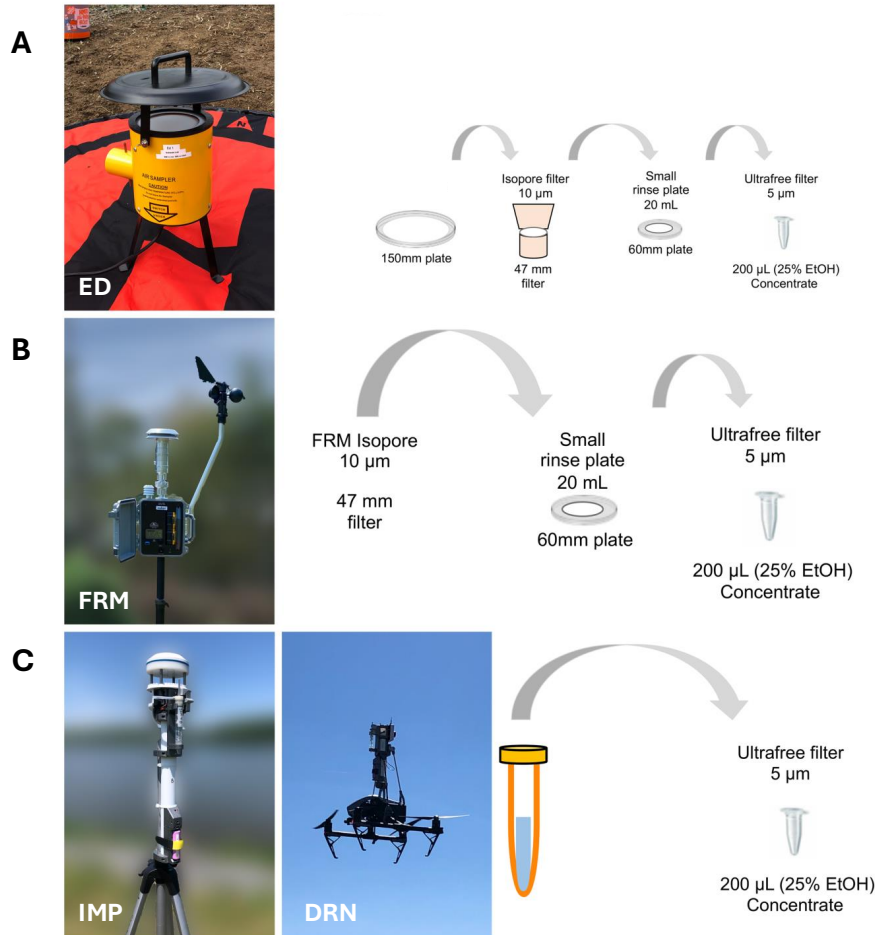


Fig. 4 Flow charts showing the processing of the filters from (A) the ED samplers, (B) the FRM sampler, and (C) the IMP and DRN samplers.

330 August 2-3, 2022, the following averaging windows were used: 45 one-minute averaging
 331 averaging windows, 9 five-minute averaging windows, and 1 full 45-minute averaging
 332 window. This approach allowed for assessing how different temporal resolutions of
 333 wind averaging influenced the accuracy of dispersal simulations.

334 To compute turbulence statistics for each averaging window, the average downwind
 335 direction was determined and the wind velocity data were rotated into a downwind
 336 (u) and crosswind (v) coordinate system. For each sampling interval, the means,
 337 covariances, and variances were computed for these wind velocity components, as well
 338 as temperature. Mean temperature was computed from sonic temperature using the
 339 method described in Schotanus et al. (1983) and the relative humidity values. Heat

340 flux was estimated from sonic temperature and relative humidity using the Bowen
341 ratio method from Schotanus et al. (1983). The Bowen ratio was determined using
342 the simplified method of Lin et al. (2016), which requires only mean temperature and
343 relative humidity. These turbulence statistics provided the necessary meteorological
344 inputs for the dispersal simulation in each interval, specifically friction velocity (u_*)
345 and the Monin-Obukhov length (L).

346 2.5.2 Pollen dispersal simulations

347 To simulate switchgrass pollen dispersal, we use the surface-layer Lagrangian Stochastic
348 (LS) model described in Aylor and Flesch (2001) and expanded to three-
349 dimensional transport in Aylor (2017). The LS model framework is based on Brownian
350 motion theory, modeling turbulent diffusion by simulating the trajectories of thousands
351 of particles through the air as random walks through the atmosphere. The movement
352 of each particle is governed by turbulent wind statistics, and the ensemble average
353 of these trajectories provides estimates of pollen concentration at any given location
354 within the simulation domain.

355 LS models require turbulent wind statistics to be specified at every point in the
356 simulation domain, including mean velocities, variances, and covariances of the wind
357 components. Under the assumptions of stationarity and horizontal homogeneity, these
358 wind field statistics remain constant over time within each averaging window but vary
359 with height. To account for this height dependence, boundary layer scaling techniques
360 are applied to generate vertical wind profiles based on measurable surface-level param-
361 eters, specifically the friction velocity (u_*) and the Monin-Obukhov length (L). The
362 full model formulation and wind statistics used in the simulations are included in the
363 code provided online.

364 These two parameters (u_* and L) were computed from the time-averaged mete-
365 orological measurements for each 45-minute sampling interval, using three different
366 averaging approaches: one 45-minute averaging window; nine 5-minute averaging win-
367 dows; and forty-five 1-minute averaging windows. A separate simulation was conducted
368 for each averaging window in a 45-minute sampling interval, using the computed
369 average wind direction, friction velocity (u_*), and Monin-Obukhov length (L). The
370 resulting concentration fields from these simulations were then averaged to generate
371 a single mean concentration field for each 45-minute sampling interval.

372 In each simulation, 100,000 particles (representing switchgrass pollen) are released
373 from a point source at the center of the field at a height of 2 m, which approximates
374 the height of most of the switchgrass panicles in the field experiment. Particles were
375 removed from the simulation domain when they: traveled more than 50 m laterally
376 from the source; rose above 100 m above ground level; or fell below 0.1 m above ground
377 level. To simplify the simulation, pollen dispersion was modeled as if it occurred over a
378 flat, rough surface, with estimated surface roughness of 0.01 m, consistent with values
379 reported for level grassy plains and prairie in Hansen (1993). The settling velocity was
380 estimated as **0.0371** m/s, based on an observed switchgrass pollen diameter of ~ 35
381 μm , using Stokes' law. Since switchgrass pollen was observed to be nearly spherical,
382 Stokes' law provides a reliable approximation of its settling velocity.

383 **2.5.3 Concentration estimation and source emission rate**
384 **calculation**

385 The pollen concentration estimation procedure in this study follows the approach
386 described by Flesch et al. (1995) for a stationary LS model with a constant source.
387 Pollen concentration is estimated by tracking the amount of time particles spend in
388 each grid box, normalized by the total number of particles released (N_p) and the
389 volume of the grid box ($V_{\text{box}} = 1 \text{ m} \times 1 \text{ m} \times 1 \text{ m}$), and then multiplied by the
390 modeled emission rate (Q). Specifically, the concentration at a given grid point (i, j, k)
391 is calculated as,

$$C(i, j, k) = Q \frac{1}{V_{\text{box}}} \frac{1}{N_p} \sum_{n=1}^{N_p} T_n(i, j, k), \quad (1)$$

392 where $T_n(i, j, k)$ represents the time particle n spends in the given grid box.

393 We employed a model-measurement fusion approach described in Aylor and Flesch
394 (2001) to estimate pollen emission rate and concentration. For each sampling interval,
395 the modeled pollen concentration at each grid point in the simulation domain is first
396 computed under the arbitrary assumption of a constant release rate at the center of
397 the field of $Q_{\text{model}} = 1$ particle per second. This yields a modeled relative concentra-
398 tion, which is proportional to the actual concentration at every point in the domain.
399 To estimate the actual emission rate (pollen flux from the field), the ratio of the mea-
400 sured pollen concentration at each of the six ED samplers to the modeled relative
401 concentration at the corresponding locations in the simulation domain was computed
402 and used to update the value of Q . To obtain a single emission rate estimate for each
403 sampling interval, the computed emission rates corresponding to calculations based on
404 each of the six ED samplers were averaged. This estimated true emission rate was then
405 used to update the modeled relative concentration to predict the actual concentration
406 at every point within the simulation domain.

407 To investigate dispersal at greater distances—up to 1 km from the source—the
408 same modeling procedure is conducted but with a coarser grid resolution of $V_{\text{box}} =$
409 $3 \text{ m} \times 3 \text{ m} \times 1 \text{ m}$ and an extended simulation domain covering $1000 \text{ m} \times 1000 \text{ m}$
410 $\times 100 \text{ m}$. This coarser grid was selected to balance computational efficiency while
411 maintaining consistency with the finer-resolution near-source grid.

412 To generate 2D dispersal kernels, which represent pollen concentration as a function
413 of distance, concentrations at equal radial distances from the source are averaged,
414 yielding average concentration as a function of radial distance from the source.

415 **3 Results**

416 **3.1 Field Experiments**

417 **3.1.1 First campaign (October 7-8, 2021)**

418 The first field campaign took place on October 7-8, 2021. At this time, the pANIC10A
419 and PSYBIN1a plants (Fig. 1) were only 11 and 6 weeks old, respectively, and the

420 youngest 200 pANIC10A plants had not yet been planted. The following ground-based
421 samplers were placed radially around the field at distances of 0, 5, 15, and 25 meters,
422 as shown in Figure 3: three ED samplers, three IMPs, and one FRM sampler. These
423 ground-based samplers operated in 30-minute intervals, while the drone-based sampler
424 (DRN) was flown at a 10-meter height for a duration of 10 minutes per sampling
425 interval. However, due to technical difficulties, the drone sampler was only deployed
426 on October 7th, and was not used on October 8th.

427 IMP A was placed at the center of the field (the midpoint of field 1 and 2) to esti-
428 mate pollen emission rate, but an insufficient amount of pollen was collected—at most
429 two pollen grains in each sampling interval, and often zero—which was not statistically
430 significant to estimate the pollen emission rate. IMP B and ED C were co-located to
431 verify alignment of their concentration estimates. However, due to their vastly differ-
432 ent sampling rates and the low pollen numbers collected, direct comparisons were not
433 feasible. On October 8th, slightly more pollen was captured, particularly by ED C,
434 but overall pollen collection remained low. Impingers showed an increase in measured
435 concentrations later in the afternoon, though data remained sparse. The IMP, FRM,
436 and DRN samplers captured negligible pollen amounts.

437 Pollen concentrations for each sampling interval and sampler are presented in Table
438 1. On October 7th, too few pollen grains were collected for meaningful analysis. Con-
439 centrations marked with a dagger[†]superscript denote cases where only 1-2 pollen grains
440 were sampled. On October 7th, all samplers captured 2 or fewer pollen grains. On
441 October 8th, 1-5 grains were collected per sampler. IMP B did not capture any pollen,
442 despite being placed alongside ED C, likely due to the overall low pollen counts.

443 3.1.2 Second campaign (October 20-21, 2021)

444 During the second field campaign on October 20-21, 2021, we increased ground-based
445 sampling intervals to 90 minutes to compensate for the low pollen counts observed
446 during the previous campaign’s 30-minute sampling intervals. To improve pollen cap-
447 ture, all samplers were moved within 15 meters of the field. The drone was still flown
448 for 10 minutes per sampling interval. On October 21st, heavy rainfall forced us to
449 shorten the final sampling interval of the day. Despite the longer sampling durations
450 and closer sampler placement, pollen counts remained negligible (at most two pollen
451 grains captured per interval) throughout this campaign. See Table 1 for details.

452 3.1.3 Third campaign (August 2-3, 2022)

453 The third and final campaign took place on August 2-3, 2022. Field and sampler
454 placements during this campaign are shown in Figure 1A and B, respectively. The
455 oldest pANIC10A plants were at peak pollen production during this campaign, but
456 the PSYBIN1a plants had not yet begun releasing pollen. The youngest pANIC10A
457 field, planted only six weeks prior, was too immature to release pollen. Given that ED
458 samplers were the most effective in previous campaigns, their number was increased
459 from three to six. In anticipation of prevailing winds directed toward north-northeast,
460 samplers were primarily aligned along the x and y axes in Figures 1 and 3. The drone
461 sampler was again flown for 10 minutes at 10 meters during all sampling intervals. ED
462 D and IMP A were co-located to compare concentration measurements. IMP B was

463 placed at the field center to estimate the pollen emission rate, if sufficient pollen was
464 collected. To address diurnal trends, sampling intervals were kept consistent across
465 both collection days. All ground-based samplers were operated for 45-minute sampling
466 intervals. ED samplers collected significantly more pollen than in previous campaigns.
467 A clear diurnal pattern emerged, with concentrations peaking between 2:00-2:45 PM
468 time on both days. Concentrations began increasing around 1:00 PM, peaked at 2:00
469 PM, then declined after 3:00 PM. See Table 1 for details.

Table 1 Pollen concentrations (pollen/m³) sampled during specific time periods, organized by date and sampler type.

Date	Time	ED						FRM	IMP			DRN**
		A	B	C	D	E	F		A	B	C	
7 Oct 2021	11:30-12:00	0	0.17	0	-	-	-	0	0	-	0	0
	12:35-13:05	0	0	0.06 [†]	-	-	-	0	0	0	0	0
	13:45-14:15	0.06 [†]	0	0	-	-	-	0	0	0	0	0
	14:45-15:15	0.11 [†]	0	0.11 [†]	-	-	-	2.00 [†]	0	0	0	0
	15:50-16:20	0.17	0.06 [†]	0.11 [†]	-	-	-	0	0	0	0	0
8 Oct 2021	12:00-12:30	0	0	0.33	-	-	-	2.00 [†]	0	0	0	-
	13:00-13:30	0.17	0.17	0.06 [†]	-	-	-	0	0	0	0	-
	14:00-14:30	0	0	0.22	-	-	-	0	111.11 [†]	0	0	-
	15:00-15:30	0.11 [†]	0.17	0.33	-	-	-	0	0	0	0	-
20 Oct 2021	14:00-16:00*	0.02 [†]	0.02 [†]	0.02 [†]	-	-	-	0.67 [†]	0	0	0	0
	16:30-18:15*	0.02 [†]	0.02 [†]	0.02 [†]	-	-	-	0	0	0	0	0
21 Oct 2021	12:00-13:45*	0	0	0.02 [†]	-	-	-	0	0	0	0	0
	14:00-14:50	0	0	0.03 [†]	-	-	-	0	0	0	0	0
2 Aug 2022	10:00-10:45	0.37	0.48	2.48	0.15	0.04 [†]	0.04 [†]	0	0	0	0	0
	11:00-11:45	0.11	0.89	0.59	0.04 [†]	0.04 [†]	0.04 [†]	0	0	0	0	0
	12:00-12:45	0.07 [†]	3.19	1.04	0.37	0.22	0.11	0	0	0	0	0
	13:00-13:45	0.22	4.30	31.78	0.33	0.26	1.89	0	0	0	0	-
	14:00-14:45	0.37	41.44	19.74	4.67	1.00	1.59	15.97	74.07 [†]	37.04 [†]	0	166.67 [†]
3 Aug 2022	15:00-15:45	0.26	5.41	5.85	0.15	0.11	0.22	3.99	0	0	37.04 [†]	0
	10:00-10:45	0.04 [†]	0.15	0.33	0	-	0.07 [†]	0	0	37.04 [†]	0	333.33 [†]
	11:00-11:45	0	1.74	0.30	0.07 [†]	0	0.15	0	0	0	0	0
	12:00-12:45	0	0.48	0.85	0.04 [†]	0.15	0.07 [†]	0	0	0	0	0
	13:00-13:45	0.15	6.22	17.89	0.74	0.04 [†]	0.11	1.33 [†]	0	37.04 [†]	37.04 [†]	0
14:00-14:45	15.11	23.44	29.26	9.67	1.70	3.19	10.65	0	444.44	74.07 [†]	500.00	
15:00-15:45	0.78	5.19	9.07	1.44	-	0.48	13.31	111.11	185.19	37.04 [†]	0	

[†] Only 1-2 pollen grains were sampled.

* For these sampling intervals, sampling times for ED and FRM were limited to two 45 minute intervals with a break in between to prevent overheating, resulting in 90 minutes of total sampling time. Impingers sampled for the entire time.

** Drone was sampling for a total of 10 minutes in each sampling interval due to battery limitations.

470 3.2 Orange-Fluorescent Protein Expression

471 The primary source of pollen in the field experiments came from the first planted block
472 of GE switchgrass, which contained 100 plants expressing OFP under the control of a
473 maize ubiquitin promoter (PvUBI1). As shown in Figure 5, the OFP signal in pollen
474 grains from these transgenic plants was difficult to distinguish from wild-type (WT)
475 pollen exposed to the same OFP-inducing wavelength of light. In contrast, the OFP
476 signal in pollen from the later planting of GE switchgrass (expressing OFP under a
477 maize pollen-specific promoter, Zm13) was much stronger and easily distinguishable
478 from WT pollen. However, these Zm13-expressing plants were smaller and did not
479 produce sufficient mature panicles in time for the field experiments, limiting their
480 contribution to the study.

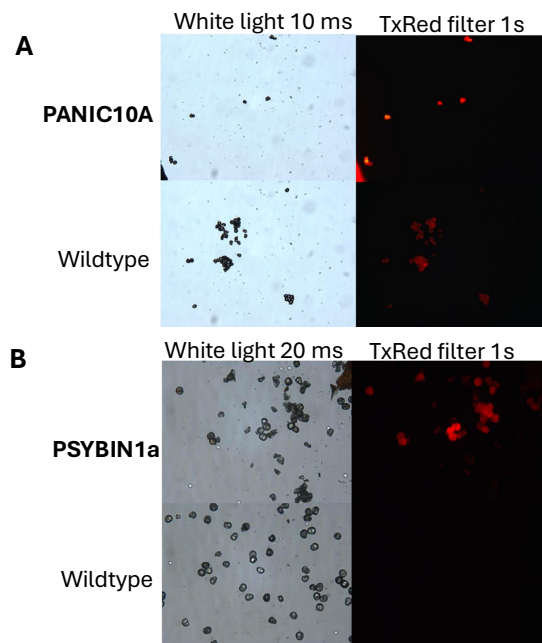


Fig. 5 Comparison of OFP signal between GE switchgrass pollen and wild-type. (A) Pollen from the pANIC10A strain (OFP expression throughout the entire plant) is not easily distinguishable from wild-type pollen under OFP-inducing light. (B) Pollen from the PSYBIN1a strain (OFP expression restricted to pollen) exhibits a strong, highly distinguishable OFP signal compared to wild-type pollen.

481 3.3 Modeling Results

482 For the dispersal modeling, we focused on the third field campaign (August 2-3, 2022),
483 as sufficient pollen was captured on both days to allow for concentration measurements
484 from the ED samplers. All sampling intervals during these days were 45 minutes long.

485 Sampling occurred at consistent times across both days, facilitating comparisons and
486 enabling the identification of diurnal trends.

487 3.3.1 Near-source concentration and emission rate estimation

488 Dispersal simulations more accurately capture changing wind directions and pollen
489 concentrations when shorter averaging periods are used for each sampling interval.
490 Figure 6 presents ground level relative concentration contours and downwind wind
491 roses for the August 2nd, 2:00-2:45 PM sampling interval, simulated using 1-minute,
492 5-minute, and 45-minute averaging windows. This interval corresponded to the highest
493 measured pollen concentrations by the ED samplers. The wind rose in Figure 6A was
494 generated using wind data collected at a sampling frequency of 10 Hz. The wind roses
495 in Figure 6B, C, and D were created using 1-minute, 5-minute, and 45-minute time-
496 averaged wind data, respectively. Wind roses display the downwind direction. Yellow
497 circles indicate the ED sampler locations, with their size proportional to pollen counts
498 at each site.

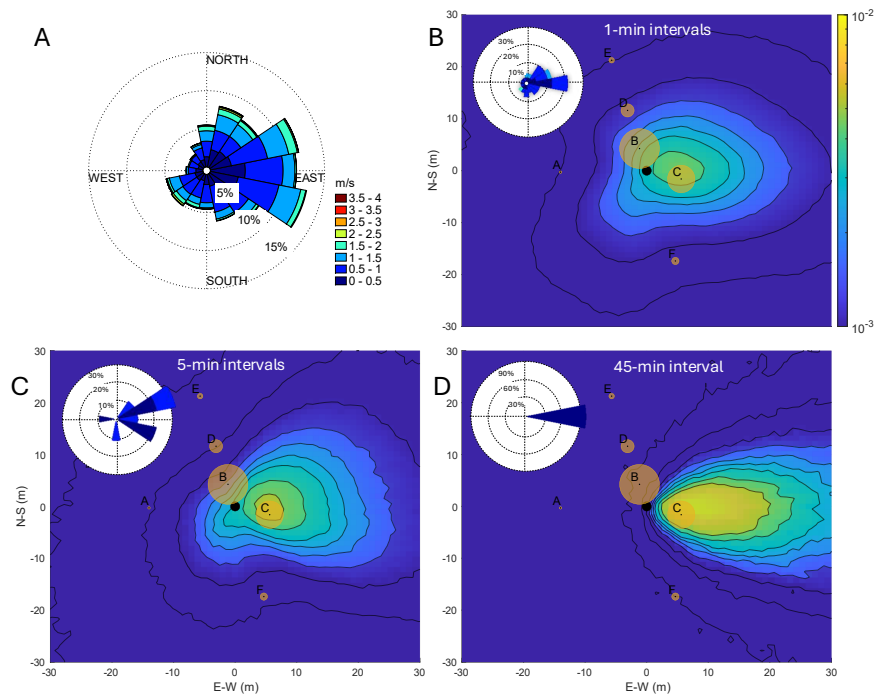


Fig. 6 Relative ground level concentration contours for the August 2nd, 2:00-2:45 PM sampling interval. (A) Wind rose for this sampling interval, indicating the downwind direction. (B) Contour plot averaging forty-five 1-minute simulations. (C) Contour plot averaging nine 5-minute simulations. (D) Contour plot generated using a single 45-minute simulation. Yellow circles indicate the ED sampler locations, with their size proportional to pollen counts at each site.

499 *Comparison of averaging windows.* The 45-minute plot (Figure 6D), based on a single
500 LS simulation in the average downwind direction, fails to capture wind variability
501 and lateral pollen spread, missing high pollen counts at ED sampler B due to a single
502 eastward-directed plume. The 5-minute plot (Figure 6C), which averages nine LS
503 simulations, shows some directional variation but lacks the detail seen in the 1-minute
504 plot. The 1-minute plot (Figure 6B) provides the most accurate representation of dispersal
505 dynamics. However, all three simulations share a common discrepancy: peak
506 concentrations appear a few meters from the point source, indicating lateral transport
507 before deposition. A field source, rather than a point source, may better address these
508 inconsistencies, albeit at the cost of further model complexity.

509 *Emission rate and diurnal pattern.* The computed pollen emission rate from the
510 field exhibits a clear diurnal trend. Figure 7 presents the mean, minimum, and maximum
511 non-zero computed emission rates for each sampling interval on August 2-3,
512 2022 during the third field campaign. Emission rates were computed from Equation
513 (1), based on the ratio of measured to modeled concentrations. Samplers with zero
514 measured or modeled concentrations were excluded to prevent infinite or zero emission
515 rate estimates. Emission rate calculations were performed for 1-minute, 5-minute,
516 and 45-minute averaging windows. The range of estimated emission rates decreases
517 with smaller averaging windows, indicating greater precision with shorter averaging
518 periods. The pollen emission rate increased by approximately three orders of magnitude
519 between 10 AM and 2 PM. Note that the emission rate is shown on a log scale in
520 Figure 7. The log-transformed emission rate estimate is positively correlated with the
521 horizontal velocity magnitude (Pearson's $R = 0.73$, $P = 0.01$), temperature ($R = 0.71$,
522 $P = 0.01$), and vapor pressure deficit ($R = 0.69$, $P = 0.01$), while negatively correlated
523 with relative humidity ($R = -0.63$, $P = 0.02$). These results indicate that higher
524 pollen emissions occur under conditions of higher wind speed, temperature, and vapor
525 pressure deficit, while increased relative humidity reduces pollen release.

526 Modeled concentration predictions improve dramatically when changing wind
527 conditions are incorporated into the simulations. Figure 8 compares modeled concentrations,
528 computed by multiplying the estimated emission rate by the relative concentration,
529 with measured concentrations derived from ED sampler pollen counts. Although the figures
530 directly compare modeled and measured concentrations, they are not intended as a formal
531 model validation, as the measured concentrations were directly used to compute emission
532 rate and modeled concentration (see Section 2.5.3). Instead, they highlight the substantial
533 improvement in model performance as the averaging window is reduced. The Pearson's
534 R -value increases from 0.19 for 45-minute windows to 0.71 for 5-minute windows to
535 0.84 for 1-minute windows. While reducing the averaging window from 45 minutes to
536 5 minutes requires nine times the computational power, it yields a 270% improvement
537 in model performance (as measured by the R -value). In contrast, refining the resolution
538 further from 5-minute to 1-minute windows results in only a 20% increase, suggesting
539 that shorter windows may not always be computationally worthwhile beyond a certain
540 threshold.

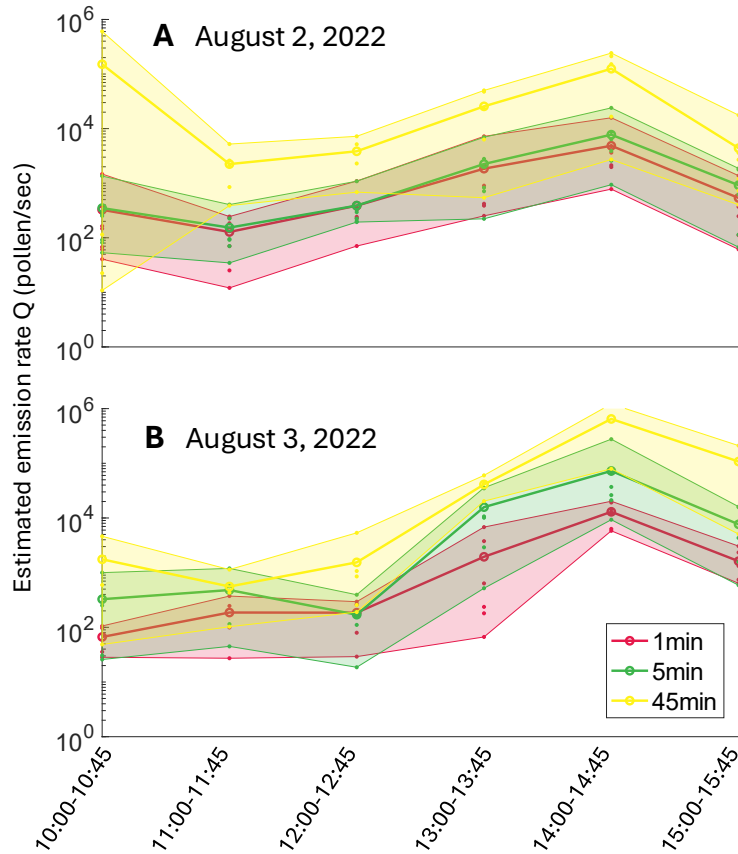


Fig. 7 Mean estimated pollen emission rates for each sampling interval using 1-minute, 5-minute, and 45-minute simulations. (A) Estimated emission rates for August 2, 2022 and (B) August 3, 2022. Non-zero emission rate estimates for each sampler are shown as solid points. Shaded regions indicate the range between the minimum and maximum non-zero emission rate estimates. The vertical axis is on a log scale.

541 3.3.2 Estimating sensor capabilities in the far field

542 The intake rates of the samplers used in this study differ by multiple orders of
 543 magnitude, with 0.6 L/min for the low-volume IMP and DRN, 16.7 L/min for the
 544 medium-volume FRM, and 600 L/min for the high-volume ED. This disparity high-
 545 lights the coarseness of concentration measurements for the low-volume IMP and DRN
 546 samplers, particularly when considering error estimates based on the Poisson distri-
 547 bution. The Poisson distribution models the error of discrete event counts, such as
 548 the number of pollen grains collected, as \sqrt{N} , where N is the number of pollen grains
 549 captured by a sampler (Addison-Smith et al. 2020; Lin et al. 2013). Lower intake

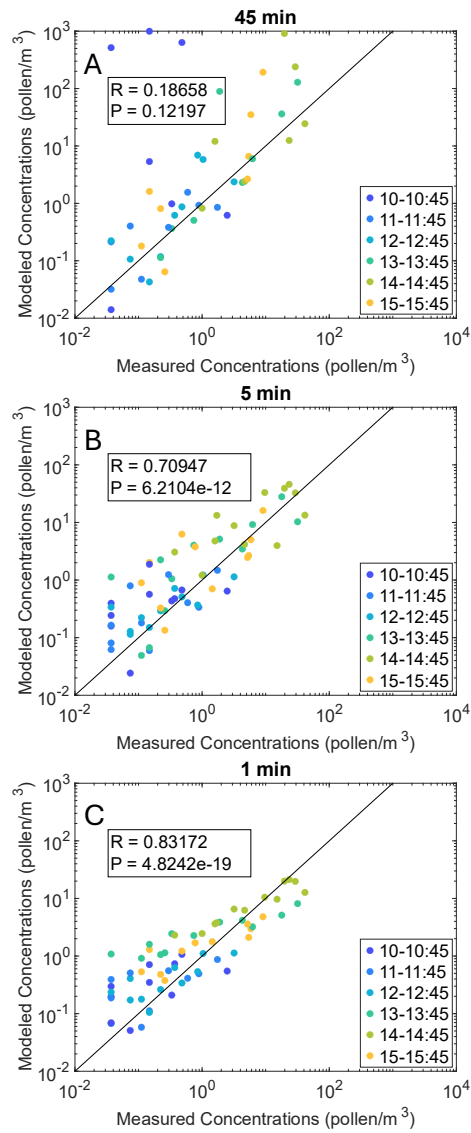


Fig. 8 Measured concentrations at the ED samplers compared with simulated concentrations for (A) 45-minute, (B) 5 minute, and (C) one-minute intervals. These plots are not intended as model validation, but rather to show that decreasing the averaging time for simulations greatly improves modeled concentrations. Note that the plots are on log-log scales.

550 rates necessitate proportionally higher aerial concentrations, and consequently, greater
 551 pollen emission rates for detection, leading to significantly higher measurement error
 552 compared to high-volume samplers.

553 To determine optimal sampler placement based on varying field emission rates, we
 554 combined sampler intake rates with long-distance dispersal simulations. Figure 9 plots
 555 the maximum distances at which each sampler could be placed to collect at least 100
 556 pollen grains (± 10) within a 45-minute sampling interval, as a function of the pollen
 557 emission rate. These estimates were generated using the long-distance 2D relative
 558 concentration dispersal kernels, computed separately for ground-based samplers (IMP,
 559 ED, FRM) at ground level and the drone-based sampler (DRN) at 10 m above ground
 560 level. Although the drone was only flown for 10 minutes per sampling interval in our
 561 field campaigns, we evaluated its performance over 45-minute intervals to account for
 562 potential future battery-life improvements or wire-tether power modifications. The
 563 threshold of 100 pollen grains corresponds to different effective concentrations across
 564 sampler types, with 3.7×10^3 pollen/m³ for IMP and DRN, 133 pollen/m³ for FRM,
 565 and 3.7 pollen/m³ for ED. This threshold was selected as it ensures a $\pm 10\%$ error in
 566 concentration estimates when modeled with the Poisson distribution.

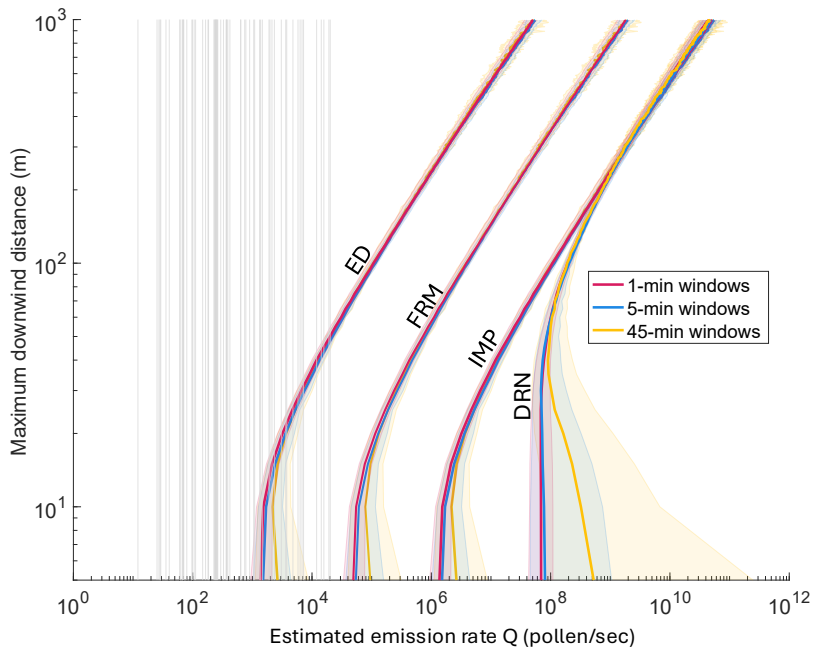


Fig. 9 Maximum distance at which ED, FRM, IMP, and DRN sensors should be placed from the source to capture at least 100 pollen grains for a given emission rate from the field. These are calculated using concentration curves derived from each sampling interval, distinguishing between estimates computed with 1-minute, 5-minute, and 45-minute averaging windows. Solid lines represent the median values, while the shaded regions indicate the range between the lowest and highest values observed across all sampling intervals. Gray vertical lines correspond to the estimated emission rates for each sensor during all sampling periods.

567 Figure 9 shows that, to collect at least 100 pollen grains, the ED samplers require
568 1.5 orders of magnitude less emission rate than the FRM and 3 orders of magnitude
569 less than the IMP, across all distances from the field. This advantage allows ED sam-
570 plers to be placed significantly farther from the field compared to IMP and FRM
571 samplers. The DRN requires an even greater emission rate, due to lower concentrations
572 at 10 meters altitude. However, at approximately 200 meters downwind, the DRN and
573 IMP detection capabilities converge, as vertical concentration gradients become less
574 pronounced further from the source.

575 The gray vertical lines in Figure 9 represent computed emission rate values at each
576 ED sampler during our field campaign, which are also shown in Figure 7. These results
577 indicate that only the ED samplers had a reasonable chance of collecting at least
578 100 particles during some sampling intervals. The remaining samplers were largely
579 ineffective at detecting airborne pollen given the small emission rates observed in
580 this study, even at close proximity to the source field. For a larger source, with an
581 emission rate of 10^6 pollen/s (approximately 100 times larger than ours), the feasible
582 placement of samplers would improve substantially. Under such conditions, impingers
583 could be placed up to 10 meters from the field, the FRM samplers could be placed
584 up to 100 meters from the field, and ED samplers could be placed up to 200 meters
585 away. These adjustments would allow each sampler type to collect at least 100 pollen
586 grains within a 45-minute sampling interval, enhancing measurement reliability and
587 reducing uncertainty.

588 4 Discussion

589 In these field experiments, airborne pollen from two different strains of OFP-expressing
590 switchgrass plants was captured and analyzed using the method described in (Rice
591 et al. 2013). The PSYBIN1a strain exhibited strong fluorescence compared to wild-
592 type pollen, whereas the pANIC10A strain was difficult to distinguish by fluorescence
593 alone. However, since the PSYBIN1a plants did not release sufficient pollen during
594 any of the field experiments, OFP expression was not used for pollen identification in
595 this study. If we had successfully captured PSYBIN1a pollen from the younger field,
596 it would have expedited the counting and sampling process. Despite this limitation,
597 the study serves as a proof-of-concept that fluorescence tagging can be a valuable tool
598 for pollen tracking. Though prior studies have tracked the movement of GE pollen
599 in the atmosphere (Aylor et al. 2006; Aylor and Flesch 2001; Aylor et al. 2003; Mill-
600 wood et al. 2017; Frisk et al. 2023), to our knowledge, this is the first detailed study
601 to incorporate aerial and ground-based volumetric samplers to track the movement of
602 GE pollen from a known source. Fluorescent tagging presents a unique opportunity
603 to trace pollen dispersal and track its movement over long distances. Understanding
604 switchgrass gene flow is particularly relevant as biofuel production increases, helping
605 to mitigate ecological risks posed by invasive strains and unintended cross-pollination
606 between transgenic varieties (Kwit and Stewart 2012). Additionally, fluorescence-
607 tagged pollen could facilitate rapid and automated counting using instruments such as
608 the Helmut Hund BAA500, Plair Rapid-E, Swisens Poleno, or WIBS-4 (Buters et al.
609 2024; O'Connor et al. 2014), which is of particular interest for allergen monitoring.

610 During the final campaign on August 2-3, 2022, a distinct diurnal pattern emerged
611 in both measured pollen concentrations and computed pollen emission rate. Pollen
612 emission rate increased steadily after the first sampling interval at 10 AM, peaked at 2
613 PM on both days, and declined during the final sampling interval at 3 PM. This diurnal
614 pattern was consistent across both days and correlated with increasing wind velocity
615 and temperature, as well as decreasing relative humidity. Such diurnal pollen release
616 patterns are common in wind-pollinated species, where anther dehiscence is driven by
617 drying conditions such as low humidity and rising temperatures (Sofiev and Bergmann
618 2012). Similar trends have been observed in previous switchgrass field studies, where
619 peak pollen concentrations occurred in the late morning and early afternoon, followed
620 by a decline around 3 PM (Auer et al. 2016). Comparable findings in maize have
621 linked pollen release patterns to increasing vapor pressure deficit (Jarosz et al. 2005)
622 and decreasing relative humidity combined with rising wind velocity (Marceau et al.
623 2011). This information can be used to better predict peak allergen concentrations
624 and improve accuracy of large-scale air pollution models.

625 Throughout all sampling intervals and field campaigns, we observed very low wind
626 velocities (< 2 m/s) and frequent shifts in wind direction. Under these meandering
627 wind conditions, particle dispersal is primarily controlled by wind direction shifts
628 rather than turbulence (Vickers et al. 2008; Anfossi et al. 2005). Standard dispersal
629 models that assume a dominant downwind direction fail to account for this effect, often
630 producing overly narrow plumes that underestimate lateral spread. This limitation
631 is particularly characteristic of LS models (Jarosz et al. 2005; Anfossi et al. 1990)
632 and Gaussian plume models (Sagendorf and Dickson 1974) which require a single
633 downwind direction. Even more advanced modeling approaches, such as Large Eddy
634 Simulations, do not fully incorporate changing wind directions (Chamecki et al. 2009).
635 To address this, we reduced the averaging window for wind statistics from 45 minutes
636 to 5 and 1 minute, then ran dispersal models for each of these smaller intervals and
637 combined the resulting plumes. This approach dramatically improved the fit between
638 modeled and measured concentrations, enhancing emission rate estimates. Similar
639 techniques have been applied in Gaussian plume modeling with 2-minute intervals,
640 yielding significantly better agreement with measured data (Sagendorf and Dickson
641 1974). Anfossi et al. (1990) Anfossi et al. (1990) also emphasized the importance of
642 using short averaging windows for dispersal modeling, recommending intervals of only
643 a few minutes. A maize dispersal study similarly attributed discrepancies between
644 measured and modeled concentrations to wind direction variability and assumptions
645 of a dominant wind direction (Jarosz et al. 2005). Future large-scale pollen forecasting
646 and bio-confinement strategies should consider meandering wind conditions, which are
647 not currently accounted for in large-scale models (Chamecki et al. 2009).

648 The highest concentration measurements in this study came from the high-volume
649 ED samplers. The pollen source size—100 plants releasing pollen—was exceedingly
650 small compared to previous dispersal experiments in switchgrass, which involved 3,200
651 plants (Auer et al. 2016), as well as studies in maize (Jarosz et al. 2005; Aylor et al.
652 2006; Marceau et al. 2011). High-volume ED samplers performed best under these
653 small-source conditions, capturing spatial variations in concentration and diurnal pat-
654 terns. To the best of our knowledge, this is the first pollen-trapping field study to

655 utilize these samplers. Their volumetric flow rate of 600 L/min is 60 times greater
656 than that of the traditional Hirst-type samplers, which operate at 10 L/min and are
657 comparable to the FRM sampler used in this study. Due to the small pollen source,
658 the FRM sampler did not produce usable data. As the ED samplers were originally
659 designed for educational purposes, they are inexpensive and lack pre-programming
660 and other advanced features found in commercial volumetric samplers. However, their
661 simplicity and affordability make them easily deployable, and they have strong poten-
662 tial for measuring concentrations from small sources and capturing high-resolution
663 pollen dispersal patterns even in small fields.

664 A novel impinger-type particle sampler (IMP and DRN) was used in this study
665 to collect pollen, marking the first application of this integrated system for pollen
666 tracking. While previously employed for airborne microbial sampling (Powers et al.
667 2018; Bilyeu et al. 2022), this study extends its use to pollen dispersal. The IMP
668 and DRN samplers successfully collected pollen in the field, demonstrating their fea-
669 sibility for tracking pollen movement. However, due to the small source size, limited
670 pollen production, and the relatively low sampling rate of 0.6 L/min, the collected
671 pollen quantities were insufficient for reliable concentration estimates. The differing
672 flow rates between the ED and IMP samplers further complicate direct comparisons,
673 as impinger samplers inherently capture fewer particles at high concentrations due
674 to their small intake volumes. The IMP system would likely perform more effectively
675 when sampling from much larger sources, at least 100 times the size of the field used in
676 our study (Figure 9). Similarly, the drone-mounted sampler, operating at 10 m above
677 ground-level, would require a significantly larger pollen source for effective deployment
678 at further distances and altitudes. Nevertheless, the drone platform remains a valu-
679 able tool for aerobiological research, offering future opportunities for prolonged and
680 spatially resolved sampling, particularly when paired with higher-volume sampling
681 technologies, including those incorporating filter-based collection systems. Moreover,
682 impinger samplers, which preserve particles in liquid, could prove especially useful for
683 future viability and molecular studies.

684 A primary constraint in regulated transgenic pollen dispersal studies is the feasi-
685 ble scale of the pollen source. From an agricultural perspective, a 100-plant source is
686 small relative to other agricultural dispersal studies. However, in the context of per-
687 mitted flowering GE pollen dispersal, it is substantial because it requires specialized
688 propagation, isolated siting, and a stringent regulatory permitting process. Our exper-
689 imental design therefore prioritized a small, but well-contained OFP-tagged source,
690 and we structured the sampling campaign to extract the most robust insights that
691 this rare setup could support. The value of the present study is therefore not that it
692 reproduces a large agricultural pollen release, but that it establishes what is measur-
693 able and how to model it under realistic constraints that are intrinsic to transgenic
694 field experimentation.

695 With more resources, the natural next step would be a scaled-up version of this
696 same experiment focused on validation: a large, well-established source containing only
697 PSYBIN1a to maximize the OFP signal, multi-year sampling on the same dates and
698 times to quantify repeatability of diurnal emission patterns, and colocated Hirst-type
699 gold-standard samplers deployed alongside the novel samplers to provide independent

700 concentration estimates for model validation and rigorous sampler inter-comparison. A
701 substantially larger source would allow meaningful comparisons between low- and high-
702 volume samplers, with one set used to estimate the particle release rate and another for
703 validating modeled concentrations. It would also enable more effective use of impinger-
704 type samplers (IMP and DRN), which could preserve pollen for downstream viability
705 studies, although isolated siting requirements for transgenic work would continue to
706 pose limits for long-distance tracking.

707 Focusing solely on PSYBIN1a switchgrass, with its stronger OFP fluorescence
708 in pollen, could further enhance tracking accuracy via automatic fluorescence-based
709 quantification. As shown in Figure 9, these methods could enable pollen detection up
710 to 1 km or even tens of kilometers from the source. This fluorescence tagging technique
711 could also be transferable to other crops of interest. For instance, hemp is known to
712 produce copious amounts of pollen capable of long-distance dispersal, and its moni-
713 toring is increasingly relevant (Nimmala et al. 2024). If transgenic hemp lines become
714 available, similar fluorescence-based tracking methods could be applied to study its
715 pollen movement and gene flow in detail.

716 5 Conclusions

717 Three field campaigns were conducted to measure pollen concentrations around a small
718 field of genetically modified switchgrass, utilizing both traditional and novel sampler
719 types. The experiments also included a drone-mounted sampler, demonstrating the fea-
720 sibility of airborne pollen sampling at 10 meters above the field as a proof-of-concept.
721 Despite the exceedingly small source size, the high-volume ED samplers successfully
722 collected sufficient pollen to analyze spatial variations in concentration and identify
723 diurnal release patterns. This study evaluated the effectiveness of different sampler
724 types for pollen collection under varying conditions. Among the three field campaigns,
725 only the final campaign on August 2-3, 2022, produced sufficient concentration data
726 for detailed analysis and modeling. During this campaign, a clear diurnal pattern was
727 observed in the pollen concentration and, consequently, in the calculated emission
728 rate. Persistent low-wind meandering conditions were recorded throughout the cam-
729 paign, and reducing the averaging window for simulations significantly improved pollen
730 emission rate estimations by better incorporating shifting wind directions. This study
731 highlights the potential for drone-based pollen sampling and fluorescence-based GMO
732 pollen tracking. The findings provide insight into the effectiveness of different sensor
733 types with respect to source strength and sampling distance, advancing the under-
734 standing of pollen dispersal dynamics and measurement techniques. These results have
735 important implications for allergen monitoring, cross-pollination risk assessment, and
736 broader bioaerosol surveillance strategies.

737 **Statements and Declarations**

738 **Data and code availability**

739 All sampling data, modeling code, and simulation results are made available in the
740 Virginia Tech Data repository:
741 <https://figshare.com/s/54a308163b60865d55bf>.

742 **Competing interests**

743 The authors have no competing interests to declare.

744 **Funding**

745 This work is supported in part by the Biotechnology Risk Assessment Program, project
746 award no. 2019-33522-29989, from the U.S. Department of Agriculture’s National
747 Institute of Food and Agriculture.

748 **References**

- 749 Adamov S, Lemonis N, Clot B, et al (2024) On the Measurement Uncertainty of
750 Hirst-Type Volumetric Pollen and Spore Samplers. *Aerobiologia* 40(1):77–91. <https://doi.org/10.1007/s10453-021-09724-5>
751
- 752 Addison-Smith B, Wraith D, Davies JM (2020) Standardising Pollen Monitoring:
753 Quantifying Confidence Intervals for Measurements of Airborne Pollen Concentra-
754 tion. *Aerobiologia* 36(4):605–615. <https://doi.org/10.1007/s10453-020-09656-6>
- 755 Ahrens C, Ecker G, Auer C (2011) The Intersection of Ecological Risk Assess-
756 ment and Plant Communities: An Analysis of *Agrostis* and *Panicum* Species
757 in the Northeastern U.S. *Plant Ecol* 212(10):1629–1642. <https://doi.org/10.1007/s11258-011-9936-9>
758
- 759 Ahrens CW, Meyer TH, Auer CA (2014) Distribution Models for *Panicum virgatum*
760 (Poaceae) Reveal an Expanded Range in Present and Future Climate Regimes in
761 the Northeastern United States. *Am J Bot* 101(11):1886–1894. <https://doi.org/10.3732/ajb.1400047>, epub 2014 Oct 24; PMID: 25366854
762
- 763 Anfossi D, Brusasca G, Tinarelli G (1990) Simulation of Atmospheric Diffusion in Low
764 Windspeed Meandering Conditions by a Monte Carlo Dispersion Model. *Nuovo Cim*
765 C 13(6):995–1006. <https://doi.org/10.1007/BF02514787>
- 766 Anfossi D, Öttl D, Degrazia G, et al (2005) An Analysis of Sonic Anemometer Obser-
767 vations in Low Wind Speed Conditions. *Boundary-Layer Meteorol* 114(1):179–203.
768 <https://doi.org/10.1007/s10546-004-1984-4>
- 769 ARA Instruments (2016) N-FRM Sampler. <https://arainstruments.com/products/n-frm-sensor/>, product web page
770

- 771 Auer C, Meyer T, Sagun V (2016) Reducing Pollen Dispersal using Forest Wind-
772 breaks. Plant Science Articles (28). URL [https://digitalcommons.lib.uconn.edu/
773 plsc_articles/28](https://digitalcommons.lib.uconn.edu/plsc_articles/28)
- 774 Aylor DE (2017) Aerial Dispersal of Pollen and Spores. American Phytopathological
775 Society, St. Paul, MN, URL <https://books.google.com/books?id=Z4e6swEACAAJ>
- 776 Aylor DE, Flesch TK (2001) Estimating Spore Release Rates Using a Lagrangian
777 Stochastic Simulation Model. J Appl Meteorol Climatol 40(7):1196–1208. [https:
778 //doi.org/10.1175/1520-0450\(2001\)040<1196:ESRRUA>2.0.CO;2](https://doi.org/10.1175/1520-0450(2001)040<1196:ESRRUA>2.0.CO;2)
- 779 Aylor DE, Schultes NP, Shields EJ (2003) An Aerobiological Framework for Assessing
780 Cross-Pollination in Maize. Agric For Meteorol 119(3-4):111–129. [https://doi.org/
781 10.1016/S0168-1923\(03\)00159-X](https://doi.org/10.1016/S0168-1923(03)00159-X)
- 782 Aylor DE, Boehm MT, Shields EJ (2006) Quantifying Aerial Concentrations of
783 Maize Pollen in the Atmospheric Surface Layer Using Remote-Piloted Airplanes
784 and Lagrangian Stochastic Modeling. J Appl Meteorol Climatol 45(7):1003–1015.
785 <https://doi.org/10.1175/JAM2381.1>
- 786 Beggs PJ (2024) Phenology and Aerobiology, Springer Nature Switzerland, Cham,
787 pp 595–608. https://doi.org/10.1007/978-3-031-75027-4_26, URL [https://doi.org/
788 10.1007/978-3-031-75027-4_26](https://doi.org/10.1007/978-3-031-75027-4_26)
- 789 Bilyeu L, Bloomfield B, Hanlon R, et al (2022) Drone–Based Particle Monitoring above
790 Two Harmful Algal Blooms (HABs) in the USA. Environ Sci: Atmos 2(6):1351–1363.
791 <https://doi.org/10.1039/D2EA00055E>
- 792 Buters JTM, Antunes C, Galveias A, et al (2018) Pollen and spore monitoring in the
793 world. Clin Transl Allergy 8:9. <https://doi.org/10.1186/s13601-018-0197-8>
- 794 Buters JTM, Clot B, Galán C, et al (2024) Automatic Detection of Airborne Pollen: An
795 Overview. Aerobiologia 40(1):13–37. <https://doi.org/10.1007/s10453-022-09750-x>
- 796 Chamecki M, Meneveau C, Parlange MB (2009) Large eddy simulation of pollen
797 transport in the atmospheric boundary layer. J Aerosol Sci 40(3):241–255
- 798 Ecker G, Meyer T, Auer C (2013) Pollen longevity and dispersion models for
799 switchgrass. Crop Sci 53(3):1120–1127
- 800 Ecker G, Zalapa J, Auer C (2015) Switchgrass (*Panicum virgatum* L.) genotypes differ
801 between coastal sites and inland road corridors in the Northeastern US. PLoS One
802 10(6):e0130414
- 803 Flesch TK, Wilson JD, Yee E (1995) Backward-time Lagrangian stochastic disper-
804 sion models and their application to estimate gaseous emissions. J Appl Meteorol
805 Climatol 34(6):1320–1332

- 806 Frisk CA, Apangu GP, Petch GM, et al (2023) Microscale pollen release and dis-
807 persal patterns in flowering grass populations. *Science of the Total Environment*
808 880:163345
- 809 Gottwald TR, Tedders WL (1985) A spore and pollen trap for use on aerial remotely
810 piloted vehicles. *Phytopathology* 75(7):801–807
- 811 Hansen FV (1993) Surface roughness lengths. US Army Research Laboratory
- 812 Isard SA, Gage SH (2001) *Flow of Life in the Atmosphere*. Michigan State University
813 Press
- 814 Jarosz N, Loubet B, Durand B, et al (2005) Variations in maize pollen emission and
815 deposition in relation to microclimate. *Environ Sci Technol* 39(12):4377–4384
- 816 Kausch AP, Hague J, Oliver M, et al (2010) Transgenic perennial biofuel feedstocks
817 and strategies for bioconfinement. *Biofuels* 1(1):163–176
- 818 Kwit C, Stewart CN (2012) Gene flow matters in switchgrass (*Panicum virgatum* L.),
819 a potential widespread biofuel feedstock. *Ecol Appl* 22(1):3–7
- 820 Li R, Qu R (2011) High throughput agrobacterium-mediated switchgrass transforma-
821 tion. *Biomass Bioenergy* 35(3):1046–1054
- 822 Lin B, Bozorgmagham A, Ross SD, et al (2013) Small fluctuations in the recovery of
823 fusaria across consecutive sampling intervals with unmanned aircraft 100 m above
824 ground level. *Aerobiologia* 29:45–54
- 825 Lin K, Juang J, Shiu YW, et al (2016) Estimating the Bowen ratio for application in air
826 quality models by integrating a simplified analytical expression with measurement
827 data. *J Appl Meteorol Climatol* 55(4):1041–1048
- 828 Mann DGJ, LaFayette PR, Abercrombie LL, et al (2012) Gateway-compatible vectors
829 for high-throughput gene functional analysis in switchgrass (*Panicum virgatum* L.)
830 and other monocot species. *Plant Biotechnol J* 10(2):226–236. <https://doi.org/10.1111/j.1467-7652.2011.00658.x>, epub 2011 Sep 28; PMID: 21955653
- 832 Marceau A, Loubet B, Andrieu B, et al (2011) Modelling diurnal and seasonal patterns
833 of maize pollen emission in relation to meteorological factors. *Agric For Meteorol*
834 151(1):11–21
- 835 Millwood R, Nageswara-Rao M, Ye R, et al (2017) Pollen-mediated gene flow from
836 transgenic to non-transgenic switchgrass (*Panicum virgatum* L.) in the field. *BMC*
837 *Biotechnol* 17:1–10
- 838 Nimmala M, Ross SD, Foroutan H (2024) *Cannabis* pollen dispersal across the United
839 States. *Sci Rep* 14(1):20605

- 840 O'Connor DJ, Healy DA, Hellebust S, et al (2014) Using the WIBS-4 (Waveband
841 Integrated Bioaerosol Sensor) technique for the on-line detection of pollen grains.
842 *Aerosol Sci Technol* 48(4):341–349
- 843 Parrish DJ, Fike JH (2005) The biology and agronomy of switchgrass for biofuels. *Crit*
844 *Rev Plant Sci* 24(5-6):423–459
- 845 Plaza MP, Kolek F, Leier-Wirtz V, et al (2022) Detecting airborne pollen using an
846 automatic, real-time monitoring system: Evidence from two sites. *Int J Environ Res*
847 *Public Health* 19(4):2471
- 848 Powers CW, Hanlon R, Grothe H, et al (2018) Coordinated sampling of microorgan-
849 isms over freshwater and saltwater environments using an unmanned surface vehicle
850 (USV) and a small unmanned aircraft system (sUAS). *Front Microbiol* 9:1668
- 851 Powers, C. (2018) Schmale-Lab-3D-Printing-Files-Powers-et-al-
852 Frontiers-2018. GitHub repository, [https://github.com/SchmaleLab/
853 Schmale-Lab-3D-Printing-Files-Powers-et-al-Frontiers-2018](https://github.com/SchmaleLab/Schmale-Lab-3D-Printing-Files-Powers-et-al-Frontiers-2018)
- 854 Rice JH, Millwood RJ, Mundell RE, et al (2013) An orange fluorescent protein tagging
855 system for real-time pollen tracking. *BMC Res Notes* 6:1–7
- 856 Sagendorf JF, Dickson CR (1974) Diffusion under low wind-speed inversion conditions.
857 Technical memorandum erl arl-52, U.S. National Oceanic and Atmospheric Admin-
858 istration, Air Resources Laboratory, Silver Spring, MD, URL [https://repository.
859 library.noaa.gov/view/noaa/31330](https://repository.library.noaa.gov/view/noaa/31330)
- 860 Schmale III DG, Dingus BR, Reinholtz C (2008) Development and application of
861 an autonomous unmanned aerial vehicle for precise aerobiological sampling above
862 agricultural fields. *J Field Robot* 25(3):133–147
- 863 Schotanus P, Nieuwstadt F, De Bruin H (1983) Temperature measurement with a
864 sonic anemometer and its application to heat and moisture fluxes. *Boundary-Layer*
865 *Meteorol* 26:81–93
- 866 Science First (2007) 15000 High Volume Air Sampler. PDF product sheet, [https:
867 //sciencefirst.com/wp-content/uploads/2017/05/15000-High-Volume-Air-Sampler.
868 pdf](https://sciencefirst.com/wp-content/uploads/2017/05/15000-High-Volume-Air-Sampler.pdf)
- 869 Sofiev M, Bergmann KC (2012) Allergenic pollen: A review of the production, release,
870 distribution and health impacts. Springer Science & Business Media
- 871 Stockdale JN, Millwood RJ (2023) Transgene Bioconfinement: Don't Flow There.
872 *Plants* 12(5):1099. <https://doi.org/10.3390/plants12051099>, URL [https://doi.org/
873 10.3390/plants12051099](https://doi.org/10.3390/plants12051099)

- 874 Suanno C, Aloisi I, Fernández-González D, et al (2021) Monitoring techniques for
875 pollen allergy risk assessment. *Environ Res* 197:111109
- 876 Techy L, Schmale III DG, Woolsey CA (2010) Coordinated aerobiological sampling of
877 a plant pathogen in the lower atmosphere using two autonomous unmanned aerial
878 vehicles. *J Field Robot* 27(3):335–343
- 879 Tummon F, Arboledas LA, Bonini M, et al (2021) The need for Pan-European auto-
880 matic pollen and fungal spore monitoring: A stakeholder workshop position paper.
881 *Clin Transl Allergy* 11(3):e12015
- 882 Vickers D, Mahrt L, Belušić D (2008) Particle simulations of dispersion using observed
883 meandering and turbulence. *Acta Geophys* 56:234–256